# RESEARCH Open Access



# High-isolation microstrip two-port diplexer and full-duplex antenna with metamaterial-based filters

Rania Hamdy Elabd<sup>1,2</sup>, Amr H. Hussein<sup>2,3</sup> and Ahmed J. A. Al-Gburi<sup>4\*</sup>

\*Correspondence:
Ahmed J. A. Al-Gburi
ahmedjamal@ieee.org
¹Electronic and Communication
Dept, Higher Institute of
Engineering and Technology in
New Damietta, Damietta
34517, Egypt
²Electronic and Communication
Dept, Horus University, New
Damietta, Egypt
³Electronics and Electrical
Communications Engineering
Department, Faculty of
Engineering, Tanta University, Tanta,
Egypt

456 July 17 Sepandoni Dan Kolumutaraan

Egypt

Fakulti Teknologi Dan Kejuruteraan
Elektronik Dan Komputer (FTKEK),
Center for Telecommunication
Research & Innovation (CeTRI),
Universiti Teknikal Malaysia Melaka
(UTeM), Jalan Hang Tuah Jaya,
76100 Durian Tunggal, Malaysia

## **Abstract**

This article presents an efficient and novel design of a microstrip three-terminal diplexer and a two-port full-duplex antenna system incorporating metamaterialbased filtering techniques to achieve high isolation and low insertion loss. Conventional diplexers and full-duplex antennas often suffer from excessive insertion loss, strong mutual coupling, and insufficient isolation, which limit their performance in modern wireless communication systems. To address these challenges, a compact 100×25.5 mm<sup>2</sup> diplexer is designed using a T-junction combiner to integrate two square open-loop resonator (SOLR)-based band-pass filters (BPFs) tuned to distinct frequencies. To enhance isolation and minimize undesired substrate coupling, metamaterial-inspired structures—specifically, four defected ground structure (DGS) cells and complementary square ring resonator (CSRR) BPFs—are incorporated. These engineered components effectively suppress surface wave propagation, enhance selectivity, and mitigate unwanted interference, resulting in superior isolation performance. Consequently, the diplexer achieves exceptional port isolation levels of -65 dB and -90 dB, with identical fractional bandwidths of 2.5%, and low insertion losses of -1.09 dB and -1.13 dB at the transmission (2.51 GHz) and reception (2.81 GHz) frequencies, respectively. To further enhance system functionality, the diplexer is integrated with a wideband Mickey-shaped patch antenna featuring a partial ground plane, ensuring bidirectional radiation, stable gain, and efficient impedance matching. The performance of the proposed system is validated through full-wave simulations and experimental measurements, showing strong agreement between theoretical and measured results.

**Keywords** Band-pass filters (BPFs), Metamaterial, Complementary square ring resonator (CSRR), Defected ground structure (DGS), Microstrip diplexer, Full-duplex

## 1 Introduction

During contemporary years, a growing amount of research has been concentrated on the enlargement of small, high-efficiency, and low-cost base stations for wireless communication technologies all over the world. Likewise, a transceiver with full-duplex is an essential mode of communication that deserves special research efforts. In a transceiver



©The Author(s) 2025. **Open Access** This article is licensed under a Creative Commons Attribution-NonCommercial-NoDerivatives 4.0 International License, which permits any non-commercial use, sharing, distribution and reproduction in any medium or format, as long as you give appropriate credit to the original author(s) and the source, provide a link to the Creative Commons licence, and indicate if you modified the licensed material. You do not have permission under this licence to share adapted material derived from this article or parts of it. The images or other third party material in this article are included in the article's Creative Commons licence, unless indicated otherwise in a credit line to the material. If material is not included in the article's Creative Commons licence and your intended use is not permitted by statutory regulation or exceeds the permitted use, you will need to obtain permission directly from the copyright holder. To view a copy of this licence, visit <a href="http://creativecommons.org/licenses/by-nc-nd/4.0/">http://creativecommons.org/licenses/by-nc-nd/4.0/</a>.

Elabd et al. Discover Applied Sciences (2025) 7:1044 Page 2 of 21

with full-duplex system, instead of using two separate antennas, it may be more cost-effective to use one antenna for both transmitting and receiving signals. However, it necessitates high ports isolation, low insertion loss, and high choosiness.

Diplexers play a crucial role in modern wireless communication systems by enabling the simultaneous transmission and reception of signals at distinct frequency bands through a single antenna or system front-end. Numerous designs have been reported in the literature [1–37], focusing on improving parameters such as isolation, insertion loss, and compactness. For instance, traditional microstrip diplexers often utilize bandpass filters combined through T-junctions or parallel coupled lines to separate transmit and receive frequencies efficiently. Recent advances incorporate metamaterial-inspired structures like Defected Ground Structures (DGS) and Split Open Loop Resonators (SOLR) to enhance selectivity and reduce mutual coupling between ports [7]. Other works have explored the integration of Complementary Split Ring Resonators (CSRR) to further suppress interference and improve port isolation, achieving substantial performance improvements in compact form factors [10]. Despite these advancements, challenges remain in balancing device size, bandwidth, and insertion loss, motivating continued research into innovative filtering and integration techniques for diplexers tailored to next-generation communication systems.

Generally, Multiplexing is the process of integrating several signals onto a one channel of communication in various ways (time, spatial, code, frequency, etc.). Frequency domain multiplexing, also recognised as duplexing, necessitates the use of high-isolation filter circuitry amongst the antenna and the transmit/receive (Tx/Rx) signal chains in order to allow only signals of the correct frequency to access their respective restraints. In [1], a full duplex microstrip antenna design with a lone gear-formed radiating patch is introduced. At the transmit and receive ports of the antenna, two high selectivity band pass filters (BPF) based on omega-shaped DGS tuned at the frequency of transmitter  $f_t$ and the frequency of receiver  $f_r$  are constructed. This structure has a small frequency space ratio of r = 0.0245, It is described as the ratio amongst the Tx & Rx frequency spacing  $\Delta f = (f_t - f_r)$  and the central frequency  $(f_t + f_r)/2$ , however its isolation is less than 36 dB. In [2], a band-pass filtering-based full-duplex microstrip antenna array setup is announced. Two H-slot resonators are used to connect two dissimilarsized microstrip resonators to the two wide-band radiating patches, establishing two BPFs at the frequencies of transmitter and receiver. This design has a high selectivity and delivers respectable band isolation. Though, its isolation does not surpass 30 dB, and its frequency space ratio of r = 0.23 is relatively high. In [3], a hollow-provide backing self-diplexing Y-shaped slot antenna with quarter-mode substrate integrated waveguide (QMSIW) is developed for high-isolation. A Y-shaped slot is inserted on the upper of the rectangular substrate integrated waveguide (SIW) to provide two unequal radiating apertures for radiation at 3.9 GHz and 4.9 GHz. This design incorporates a high-gain antenna; though, it exhibits a suboptimal Tx-Rx isolation of 34 dB dB and a high-frequency space ratio represented by r = 0.227. Another approach, as described in [4], introduces a self-diplexing bow-tie shaped slot antenna utilizing a Substrate Integrated Waveguide (SIW) cavity. This cavity is stimulated by two separate feed lines, enabling resonance at both transmitting and receiving frequencies. While this well-established configuration gives a great-gain antenna with a unidirectional radiation pattern, it still suffers from a high-frequency space ratio of r = 0.22 and a Tx-Rx isolation of 22 dB. In Elabd et al. Discover Applied Sciences (2025) 7:1044 Page 3 of 21

another instance, detailed in [5], a dual-band microstrip patch antenna is presented for diplexing operations. The antenna transceiver is comprised of three layers, with an air layer squeeze in amid two stepped impedance microstrip line resonators to establish isolation between the two ports at the operating bands. Nevertheless, this antenna exhibits a high-frequency spacing ratio of r=0.7 and suboptimal isolation values of  $22\,dB$  and  $28\,dB$  in the low and high bands, correspondingly.

On the other hand, many research efforts are performed to design ultra and super wideband (SWB) antennas for diplexing purposes. In [6], a small concentric structured monopole patch antenna for SWB requests has been announced. It provided a fractional bandwidth of 190~% for  $S_{11} < -10~dB$ , and covered the frequency range from 1.22~GHz to 47.5~GHz. A similar notion was investigated in this paper for an antenna that would have a large frequency range and span two resonance frequencies.

In this work, well-organized designs for a microstrip three-terminal diplexer and a two-terminal full-duplex microstrip antenna for wireless communication technologies are introduced. Firstly, we started by the re-optimization of the size of the feeding transmission lines and the DGS cells of our published diplexer introduced in [7] to improve its selectivity, insertion loss, and isolation giving rise to the initially modified diplexer. Secondly, for further performance enhancement of the initially modified diplexer in terms of isolation and insertion loss, the complementary square ring resonator (CSRR) metamaterial technique is utilized. A group of N closely spaced CSRRs are etched along a segment of a transmission line to form a broadband CSRR-based BPF at the top-layer and in the near vicinity of the coupled square open-loop resonators (SOLRs) and the T-junction combiner of the initially modified diplexer. By adjusting the locations of the CSRR-based BPFs, they can swallow any interfering waves impinging on the diplexer and swallow the traveling waves through the substrate from port 1 to port 2 within the frequency band from  $1.5\,GHz$  to  $4\,GHz$ . This significantly reduces the coupling between the diplexer ports and improves the isolation. Accordingly, an extremely efficient diplexer with high selectivity, little insertion loss, and great isolation is developed.

The developed diplexer is integrated with a well-designed wideband antenna element that spans the frequency band from  $1.5\,GHz$  to  $4\,GHz$  to construct the proposed two-port full-duplex microstrip antenna structure with a transmit frequency of  $f_t=2.51\,GHz$  and a receive frequency of  $f_r=2.81\,GHz$ .

The proposed wideband antenna element comprises of a Mickey-shaped radiator patch with a partial ground plane. The suggested antenna is a derivative from the traditional circular monopole antenna. To achieve wide bandwidth covering the desired transmit and receive frequencies, the traditional circular monopole antenna has been adapted by connecting two circular ears at the top view of the antenna and adapting its partial ground plane similarly. The innovation in this antenna arrangement comes from the addition of three open-end transmission lines on either side of the radiator, which facilitates the extension of the impedance bandwidth of the antenna. The addition of these lines helps to growth the current path length and thus save the size of the antenna whole.

After integrating the proposed diplexer with the antenna element to construct the full-duplex antenna system, we observed that the overall system exhibited satisfactory performance. This encouraged us to further optimize the design by etching a circular defected ground structure (DGS) beneath the radiating patch and introducing a

meandered feeding transmission line. As a result, the final full-duplex Tx/Rx antenna system was developed with enhanced characteristics. It achieves a compact size of  $100 \times 70 \text{ mm}^2$ , excellent isolation of -31 dB at the transmit frequency  $f_t$ =2.51 GHz and -58 dB at the receive frequency  $f_r$  =2.81 GHz. The return losses are -32 dB and -38 dB at the transmit and receive frequencies, respectively, with a small frequency spacing ratio of r = 0.11278.

# 2 Proposed full duplex microstrip antenna system

This section introduces a novel configuration for an efficient full-duplex microstrip antenna system, commonly referred to as a duplexer, tailored for modern wireless communication applications. The duplexer operates at two distinct resonance frequencies, 2.51 GHz for transmission and 2.81 GHz for reception. The scheme and simulation of the suggested duplexer are carried out on a Rogers TMM4 substrate with a thickness of 1.52 mm and a relative dielectric constant of  $\epsilon_r=4.5$ . The simulations are performed using the CST Microwave Studio software, specifically the CST-MWS-2019 version.

The scheme methodology of the proposed duplexer is outlined in the flowchart presented in Fig. 1, which can be broken down into six key steps: (i) Designing the primary construction of the microstrip diplexer, (ii) Developing the Bandpass Filter (BPF) using

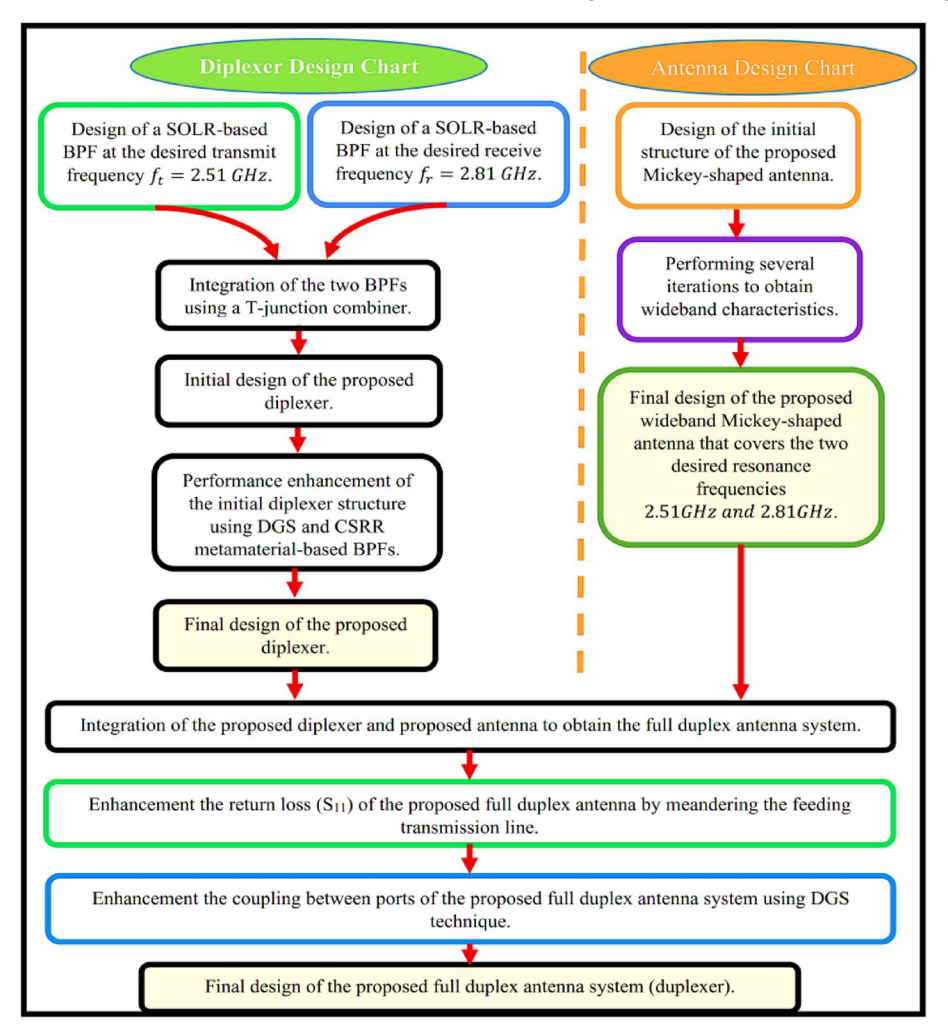


Fig. 1 The design procedure flowchart for the suggested full-duplex antenna system

Complementary Split Ring Resonator (CSRR) metamaterial, (iii) Enhancing the diplexer's performance by incorporating the CSRR metamaterial approach, (iv) Designing the proposed wideband antenna element, (v) Creating the preliminary duplexer structure, and (vi) Optimizing the duplexer's performance with the use of meandered transmission lines and the Defected Ground Structure (DGS) technique.

# 2.1 Formation of the preliminary configuration for the envisioned microstrip diplexer

Referring to our published diplexer introduced in [7], Fig. 2 (a) and (b) shows a diplexer based on utilization of DGS and coupled SOLR-based BPFs. This diplexer is made up of two SOLR- based BPFs that are integrated using a T-junction combiner. To enhance insertion loss and minimize coupling between ports, four Defected Ground Structures (DGSs) are etched into the ground plane beneath the four Split-Open Loop Resonators (SOLRs) [7]. In this study, the widths of the feeding transmission lines at ports 1, 2, and 3, as well as the dimensions of the DGS cells engraved in the ground plane, have been reoptimized to realize improved insertion loss, reduced mutual coupling between ports, and enhanced selectivity. The optimized dimensions are provided in Table 1, where they are compared with the original diplexer design from [7]. Figures 2(c) and 2(d) present the simulated scattering parameters of the optimized diplexer alongside the original design from [7]. Upon examining the results, it is evident that return losses, coupling losses, and insertion losses have been significantly improved, as indicated in Table 2, which shows the corresponding improvement ratios.

# 2.2 Design of the modelled CSRR metamaterial based BPF

In this section, a complementary split ring resonator (CSRR) filtering element using defected microstrip structure (DMS) is proposed to minimize the coupling and insertion losses. Single negative metamaterial elements such as split ring resonators (SRR) and CSRR are well-known. Pendry et al. were the first to propose a mu-negative (MNG) SRR model [8]. When Babinet's concept is applied, complimentary SRR is implemented

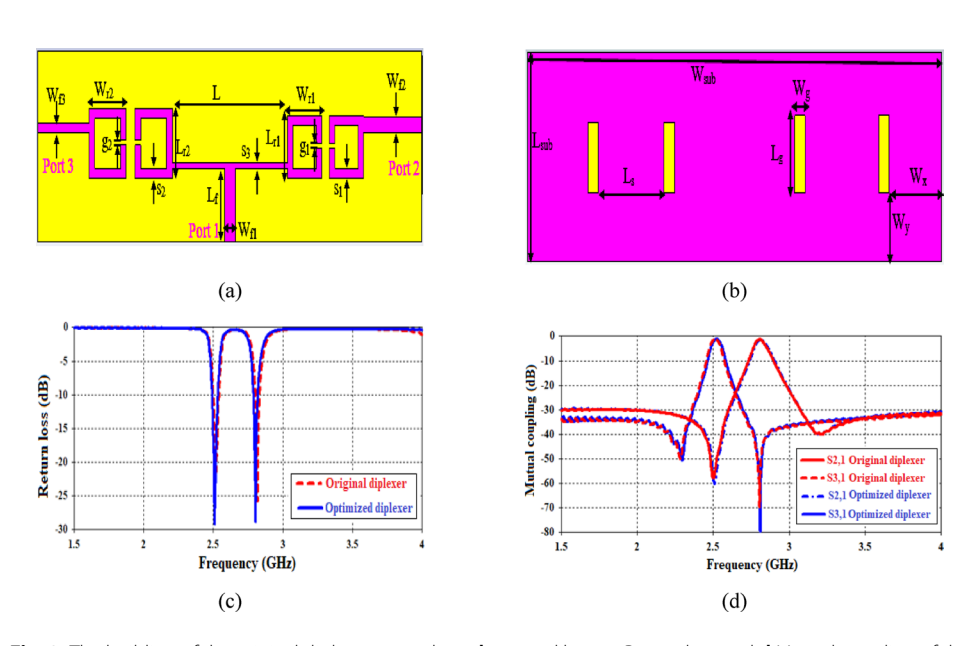


Fig. 2 The building of the original diplexer: **a** top-layer, **b** ground layer, **c** Return loss and **d** Mutual coupling of the optimized diplexer

Elabd et al. Discover Applied Sciences (2025) 7:1044 Page 6 of 21

**Table 1** The optimized dimensions in comparison to the dimensions of the original diplexer presented in [7]

Dimensio	ns that remained und	hanged		Optimized dimensions	
Symbol	Dimension (mm)	Symbol	Dimension (mm)	Symbol	Dimension (mm)
$\overline{W_{ m sub}}$	100	$W_{r1}$	9	$L_g$ (optimized)	11
				$L_g$ (old)	10.6
$L_{ m sub}$	28.5	$W_{r2}$	9.7	$W_f$ (optimized)	3.17
				$W_f$ (old)	2.8
$oldsymbol{L_{r1}}$	9.4	$g_1$	0.75	$W_{f1}$ (optimized)	2.824
				$W_{f1}$ (old)	1.4
$oldsymbol{L_{r2}}$	10.4	$g_2$	0.75	$L_s$ (optimized)	18.7
				$L_s$ (old)	17.7
$oldsymbol{S}_1$	1.5	$L_f$	11	$W_{f1}$ (optimized)	2.824
				$W_{f1}$ (old)	1.4
$oldsymbol{S}_2$	1.5	L	30	$W_{f2}$ (optimized)	2.815
				$W_{f2}$ (old)	2.4
$S_3$	0.8	$W_y$	8.95	$W_g$ (optimized)	1.875
				$W_g$ (old)	2.5
$W_x$	12.8				

**Table 2** Realized specifications of the optimized diplexer compared to original diplexer

Specifications	Original diplexer [7]	Optimized diplexer	Improvement ratios for optimized diplexer over original diplexer
Size in $(mm^2)$	$100 \times 28.5$	$100 \times 28.5$	Unchanged
$f_t$ (GHz)	2.51~GHz	2.51GHz	Unchanged
$f_r$ (GHz)	2.81~GHz	2.81~GHz	Unchanged
FBW (%)	2.8% at $2.51GHz$	2.72~% at $2.51~GHz$	2.857% at $2.51GHz$
	2.8% at $2.81GHz$	2.65~% at $2.81~GHz$	5.357~% at $2.81~GHz$
Return loss (dB)	$21\ dB$ at $\ 2.51\ GHz$	$29\ dB$ at $2.51\ GHz$	38~% at $2.51~GHz$
	$24\ dB$ at $\ 2.81\ GHz$	28dB at $2.81GHz$	16.66% at $2.81GHz$
Ports isolation (dB)	$56~dB~{\rm at}~2.51~GHz$	$60\ dB$ at $2.51\ GHz$	7.1~% at $2.51~GHz$
	$65\ dB$ at $\ 2.81\ GHz$	$80\ dB$ at $2.81\ GHz$	23~% at $2.81~GHz$
Insertion loss (dB)	1.2dB at $2.51GHz$	$1.15\ dB$ at $\ 2.51\ GHz$	4.1~% at $2.51~GHz$
	$1.3\ dB$ at $\ 2.81\ GHz$	$1.22\ dB$ at $\ 2.81\ GHz$	6.153% at $2.81GHz$

[9]. The epsilon-negative (ENG) CSRR was first hosted in [10] through the application of duality, which involved swapping the roles of metal and dielectric materials in the Split-Ring Resonator (SRR). Unlike the SRR, the CSRR exhibits reversed electrical and magnetic properties. However, both resonators typically share nearly identical resonant frequencies [10]. Consequently, the resonance frequency of the CSRR can be founded by referring to the SRR. Figure 3 demonstrates the diagram and equivalent circuit model of the CSRR. The CSRR offers several benefits, including enhanced filtering performance for coupling destruction, a compressed size, and ease of fabrication.

Figure 3(a) illustrates the general schematic illustration of an SRR unit cell, while Fig. 3(b) displays the conforming equivalent circuit model for the SRR unit cell. The equivalent circuit model for the Complementary Split Ring Resonator (CSRR) consists of a shunt LC resonator linked to the microstrip line through a capacitance ( $c_d$ ), as depicted in Fig. 3(b). This shunt resonator is a parallel combination of  $L_{net}$ , and  $c_e$ . The CSRR functions as an externally driven LC resonant circuit [11]. The resonance frequency of the CSRR unit cell is dictated by the self-inductance ( $L_{self}$ ) and capacitance

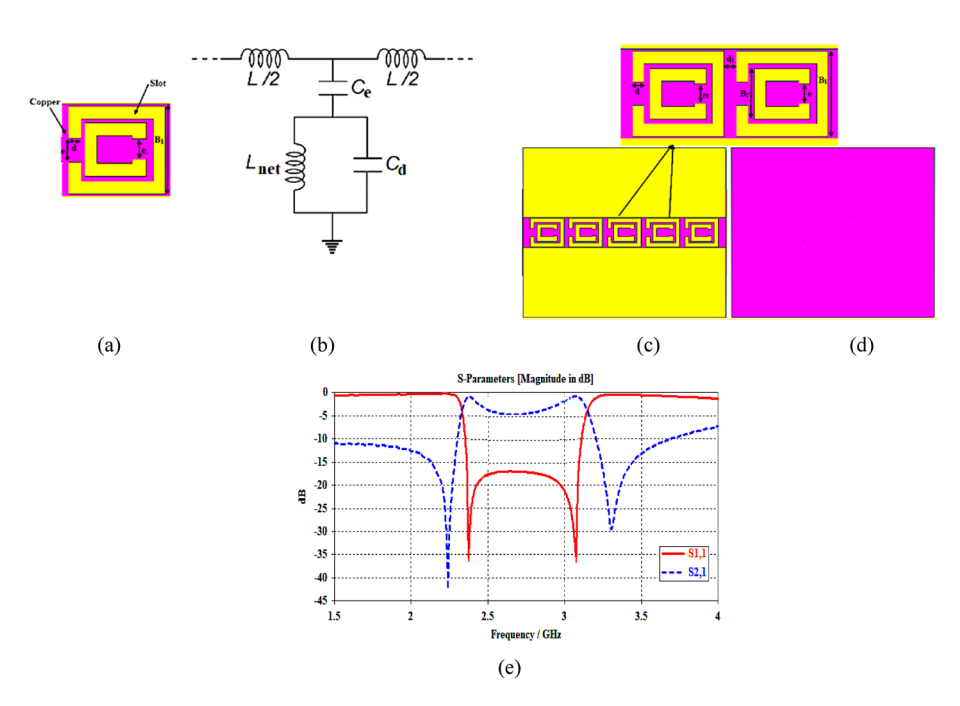


**Fig. 3** Proposed CSRR unit cell: **a** Schematic diagram, **b** Equivalent circuit model. Proposed CSRR-based BPF: **c** top-layer, and **d** ground layer, and **e** Simulated scattering parameters of the proposed CSRR-based BPF

per unit length ( $C_{pul}$ ), as outlined in [12]. The resonant frequency ( $f_0$ ) of the CSRR can be determined using the formula provided in [13]:

$$f_{0=\frac{1}{2\pi\sqrt{L_{net}C_{net}}}}.$$

Here,  $L_{net}$  represents the cumulative inductance of the structure, and  $C_{net}$  signifies the overall capacitance of the system. The total net capacitance,  $C_{net}$ , can be articulated as follows:

$$C_{net} = \frac{(c_d + c_e)}{2}. (2)$$

Here,  $c_d$  represents the series capacitance, while  $c_e$  refers to the gap capacitance. The general capacitance equation allows us to define the gap capacitance  $c_e$  as:

$$c_e = \frac{\epsilon_0 dt}{e}.$$
 (3)

In this context, d and t denote the width and thickness of the metal rings, correspondingly.  $\epsilon_0$  represents the permittivity of free space, and e refers to the dimension of the split gap.

The distributed capacitance  $c_d$  depends on the split gap dimension e and the ring dimension  $B_1$  and is expressed as follows:

$$c_s = (4B_1 - e) C_{pul}.$$
 (4)

The capacitance per unit length, denoted as ( $C_{pul}$ ), is computed as follows:

$$C_{pul} = \frac{\sqrt{\epsilon_r}}{CZ_0} \tag{5}$$

Where  $\epsilon_r$  is the effective permittivity of the medium, C is the speed of light, and  $Z_0$  is the characteristic impedance of the line. Substituting the values of  $c_d$  and  $c_e$  in (2), the net capacitance  $C_{net}$  can be rewritten as:

$$C_{net} = \left(2B_1 - \frac{e}{2}\right)C_{pul} + \left(\frac{\epsilon_0 st}{e}\right). \tag{6}$$

The complete inductance of the suggested circuit model can be determined utilizing the following relationship:

$$L_{net} = (0.0002) l \left( 2.303 log_{10} \frac{4l}{d} - \gamma \right). \tag{7}$$

In this equation,  $\gamma$  equals 2.8, which is an empirically derived constant used to account for the internal inductance and mutual coupling effects in square-loop resonators. This value has been validated and widely adopted in the literature for modelling the inductance of square CSRR structures, as referenced in [10–12]. Here, l represents the effective length of the wire forming the loop, computed as follows:

$$l = 8B_1 - d. (8)$$

Hence, the resonant frequency  $f_0$  can be determined by substituting the values of the total capacitance and inductance into Eq. (1).

In this section, a design for a broadband BPF that covers the desired transmit and receive frequencies is introduced. It is based on the CSRR metamaterial technology. In the proposed CSRR cell design, two square-shaped shaped SRRs of different sizes are constructed and nested such that their gap openings are opposite to each other to form a complementary structure as shown in Figs. 3 (c) and (d). The sizes of the suggested CSRR cell are registered in Table 3. To build up the proposed CSRR-based BPF, five CSRR cells are linearly aligned with inter cell spacing  $d_1$  as shown in Fig. 3. The virtual S-parameters of the CSRR-based BPF are presented in Fig. 3 (e). It is clear that the BPF has a broad bandwidth that ranges from  $2.4\,GHz$  to  $3.1\,GHz$ , which covers the desired transmit and receive frequencies.

# 2.3 Improving the performance of the suggested diplexer through the CSRR metamaterial technique

In this segment, the suggested CSRR-based BPF is applied to enhance the performance of the optimized diplexer in terms of isolation and insertion loss. As shown in Fig. 4 (a), two sets each consisting of five CSRR cells are etched at the top-layer near the horizontal branch of T-junction forming two broadband BPFs whose scattering parameters are represented previously in Fig. 3. By adjusting the locations of the etched BPFs, they can swallow transmit and receive frequencies that travel through the substrate from port 1 to port 2 and vice versa. Furthermore, they can swallow the other interfering frequencies

**Table 3** Dimensions of the proposed CSRR cell

Symbol	Dimension $(mm)$	Symbol	Dimension $(mm)$	
$B_1$	1.45	$B_2$	0.85	
e	0.46	$e_1$	0.275	
d	0.2	$d_1$	0.3	

Elabd et al. Discover Applied Sciences (2025) 7:1044 Page 9 of 21

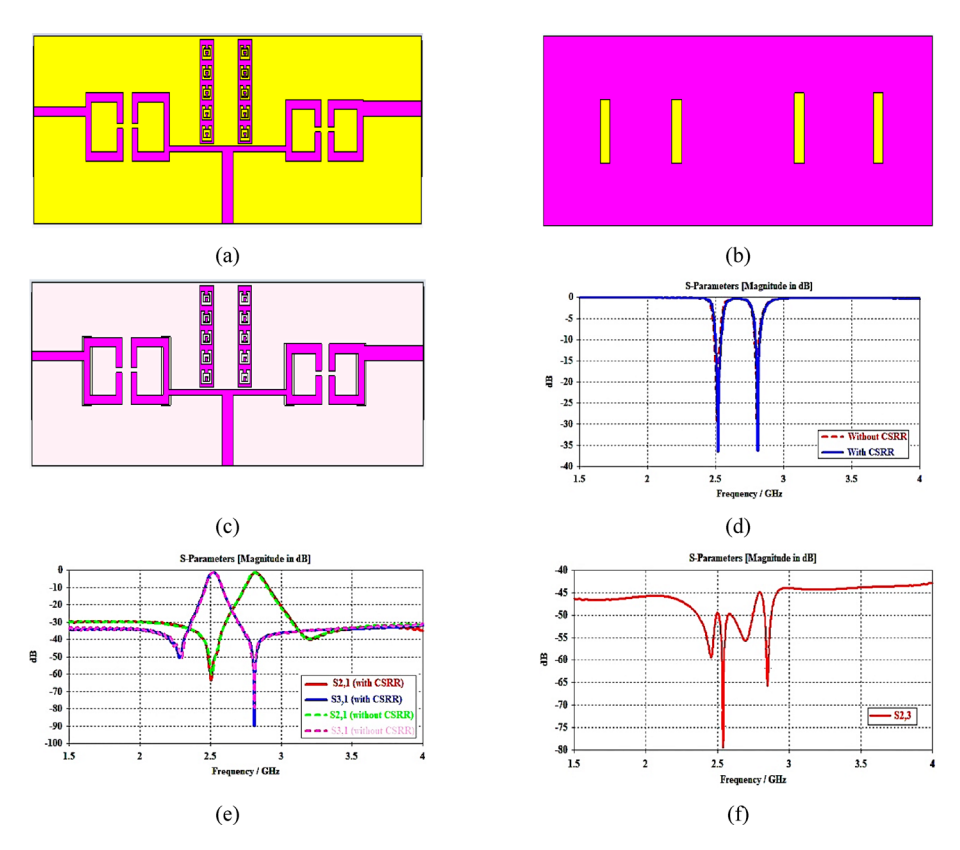


**Fig. 4** Demonstrates the ultimate configuration of the envisioned diplexer incorporating Bandpass Filters (BPFs) based on CSRRs: **a** depiction of the top layer, **b** representation of the ground layer, and **c** the conclusive construction of the diplexer. The simulated scattering parameters, including **d** return loss, **e** insertion loss, and **f** mutual coupling, are also presented for analysis

within the  $1.5\,GHz$  to  $4\,GHz$  frequency band. This indeed improves the insertion loss and selectivity of the diplexer. Figure 4 (c) shows the final scheme of the suggested diplexer, while Figures. 4 (d) and (e) show the simulated scattering parameters of the final diplexer employing CSRR-based BPFs compared to the optimized diplexer. By analyzing the results, it is found that there are significant improvements in selectivity, return loss, isolation, and insertion loss as displayed in Table 4. Compared to the original diplexer, the FBWs are improved by 10.71% for both transmit and receive frequencies. The return losses are improved by 76.19% and 50% at transmit and receive frequencies, respectively. The achieved ports isolations reached 65~dB at 2.51~GHz and 90~dBat  $2.81\,GHz$ , which are improved by 16% and  $38.46\,\%$  for the transmit and receive frequencies, correspondingly. In the same context, the realized insertion losses reached 1.09~dB at 2.51~GHz and 1.13~dB at 2.81~GHz, which are improved by 9.16~% and 13.07 % for the transmit and receive frequencies, correspondingly. On the other hand, the simulated S-parameter S23 versus the frequency for the final diplexer is presented in Fig. 4 (f) to clarify the coupling between port 2 and port 3. It is clear that they have very low coupling where the isolation between the two ports reached 80 dB and 66 dB for 2.51 GHz and 2.81 GHz, correspondingly.

# 2.4 Development of the suggested wideband antenna component

In this section, we present a novel design for a wideband Mickey Mouse-shaped antenna element. The configuration includes a radiating patch in the shape of a concentric mouse

 Table 4
 The realized specifications of the final diplexer compared to the original and optimized diplexers

	_	-	_	
Specifications	Original diplexer [7]	Optimized diplexer	Final Diplexer	Improvement ratios for final diplexer over original diplexer
Size in $\left(mm^2 ight)$	$100 \times 28.5$	$100 \times 28.5$	$100 \times 28.5$	Unchanged
$f_t$ (GHz)	2.51GHz	2.51~GHz	2.51~GHz	Unchanged
$f_r$ (GHz)	2.81GHz	2.81GHz	2.81~GHz	Unchanged
FBW (%)	2.8% at $2.51GHz$	2.72~% at $2.51~GHz$	2.5% at $2.51GHz$	10.71% at $2.51GHz$
	2.8% at $2.81GHz$	2.65~% at $2.81~GHz$	2.5% at $2.81GHz$	$10.71\ \%$ at $2.81\ GHz$
Return loss (dB)	21~dB at $2.51~GHz$	29~dB at $2.51~GHz$	37dB at $2.51GHz$	76.19% at $2.51GHz$
	24~dB at $2.81~GHz$	28~dB at $2.81~GHz$	36dB at $2.81GHz$	50% at $2.81GHz$
Ports isolation (dB)	56~dB at $~2.51~GHz$	60~dB at $~2.51~GHz$	65dB at $2.51GHz$	16% at $2.51GHz$
	65~dB at $~2.81~GHz$	80~dB at $~2.81~GHz$	$90\ dB$ at $2.81\ GHz$	38.46 % at $2.81  GHz$
Insertion loss (dB)	$1.2\ dB$ at $2.51\ GHz$	$1.15\ dB$ at $2.51\ GHz$	$1.09\ dB$ at $2.51\ GHz$	9.16% at $2.51$ $GHz$
	$1.3\ dB$ at $2.81\ GHz$	$1.22\ dB$ at $2.81\ GHz$	$1.13\ dB$ at $2.81\ GHz$	13.07 % at $2.81  GHz$

Elabd et al. Discover Applied Sciences (2025) 7:1044 Page 11 of 21

and a ground plane that is semi-circular and loaded with a notch. The ultimate geometric arrangement of the antenna element is showed in Fig. 5. For the planned antenna construction, the optimal dimensions are provided in Table 5. The substrate espoused for designing the proposed antenna is a Rogers TMM4 substrate having a thickness  $h=1.52\ mm$  and a relative dielectric constant  $\epsilon_{r}=4.5$ . The initial geometric parameters of the proposed Mickey-shaped antenna were calculated based on standard microstrip patch antenna theory. Specifically, the effective dielectric constant  $\epsilon_{eff}$ , effective length  $L_{eff}$ , and physical width and length of the radiating element were estimated using the following Eqs. (9–13):

$$\epsilon_{eff} = \frac{\epsilon_r + 1}{2} + \frac{\epsilon_r - 1}{2} (1 + 12 \frac{h}{W})^{-0.5}$$
 (9)

$$L_{eff} = \frac{c}{2f_r\sqrt{\epsilon_{eff}}} \tag{10}$$

$$\Delta L = 0.412h \frac{(\epsilon_{eff} + 0.3)(\frac{W}{h} + 0.264)}{(\epsilon_{eff} - 0.258)(\frac{W}{h} + 0.8)}$$
(11)

$$L = L_{eff} - 2\Delta L \tag{12}$$

$$W = \frac{c}{2f_r} \sqrt{\frac{2}{\epsilon_r + 1}}. (13)$$

Where:  $\epsilon_r$  is the Relative dielectric constant of the substratem, h is the Substrate thickness, c is the Speed of light in vacuum and  $f_r$  is the resonant frequency. These calculations provided a reliable starting point for the antenna topology. Subsequently, the structure was reshaped into the Mickey profile, and its critical dimensions were fine-tuned through full-wave simulations to achieve the desired bandwidth, impedance matching, and radiation characteristics.

The four progressive design phases of the suggested antenna construction are shown in Fig. 6 (a). The corresponding reflection coefficient ( $S_{11}$ ) versus frequency curves of the four antenna configurations in each of the design phases are illustrated in Fig. 6 (b).

In iteration #0, it is observed that the impedance matching is suboptimal across the entire frequency range, primarily due to the abrupt change in impedance at the junction between the coolant and the feed line.

In iteration #1, two eyes and a mouth are made in the mouse-shaped radiating patch to expand the frequency band below the -10 dB reference. In iteration #2, a notch is placed in the semi-circular ground plane to minimize the effect of capacitance, as seen below. The overall capacitance is depleted when the coupling is lowered, resulting in an increase in the resistance bandwidth.

In iteration #3, the insertion of the six open stubs at the top of the monopole increases the electrical length of the monopole and extends the bandwidth from  $2.2\,GHz$  to  $3.8\,GHz$ , attaining well impedance matching across the entire frequency range from  $2.2\,GHz$  to  $3.8\,GHz$  compared to iteration #0 as shown in Fig. 6 (b).

Upon examining the final antenna design arrangement obtained through the third iteration, the graph in Fig. 7(a) displays the realized antenna gain relative to frequency. The antenna demonstrates a substantial gain, ranging between 2.28 dB and 2.418 dB,

Elabd et al. Discover Applied Sciences (2025) 7:1044 Page 12 of 21

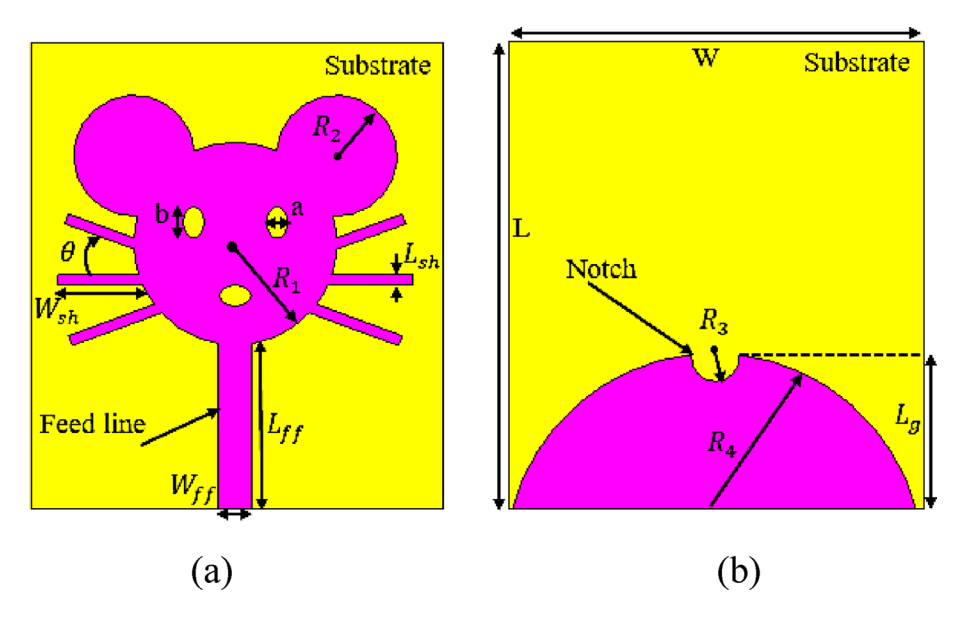


**Fig. 5** Illustrates the geometric configuration of the suggested wideband antenna element in the form of a Mickey Mouse shape. The depiction includes **a** the view from above and **b** the view from below

**Table 5** Optimal dimensions of the designed antenna

Parameter	Dimension $(mm)$	Parameter	Dimension $(mm)$	
$\overline{W}$	40	$R_2$	5.8	
L	45	$R_3$	2.3	
$R_1$	9.7	$R_4$	20	
$L_g$	10	$W_{sh}$	11	
$W_{ff}$	3.17	a	1	
$L_{ff}$	16	b	1.5	
$L_{sh}$	1	heta	20	

covering the operational frequency spectrum from 2.52 GHz to 3.82 GHz. Additionally, it exhibits high radiation efficiency, spanning from 97.8 to 96.7%, across the frequency band of 2.52 GHz to 3.82 GHz, as depicted in Fig. 7(b). In addition, the real part of the antenna's reference impedance consistently maintains a value of 50 ohms, as described in Fig. 7(c).

# 2.5 Development of the preliminary configuration for the envisioned duplexer

The primary part of a duplexer is to manage the signal flow between the transmitter and the antenna in both directions, a function that is efficiently achieved in the planned antenna system. This section introduces the primary configuration of the envisaged full-duplex Transmit/Receive (Tx/Rx) patch antenna system. It is based on the integration of the proposed diplexer introduced in Sect. (2.3) and the Mickey Mouse-shaped antenna element introduced in Sect. (2.4) as shown in Figures. 8 (a) and (b). Despite the fact that ports #3 and #2 are assigned to transmission and reception modes, respectively, the feeding transmission line of the antenna is connected to feeding port #1 of the diplexer.

A Rogers TMM4 substrate with overall dimensions of 100 mm  $\times$  70 mm  $\times$  1.52 mm, a thickness of h = 1.52 mm, a relative dielectric constant of  $\epsilon_r = 4.5$ , and a loss tangent of  $\delta$  = 0.002 is used to build the duplexer system. The simulated scattering characteristics of the first proposed Tx/Rx antenna system, with transmission and reception frequencies

Elabd et al. Discover Applied Sciences (2025) 7:1044 Page 13 of 21

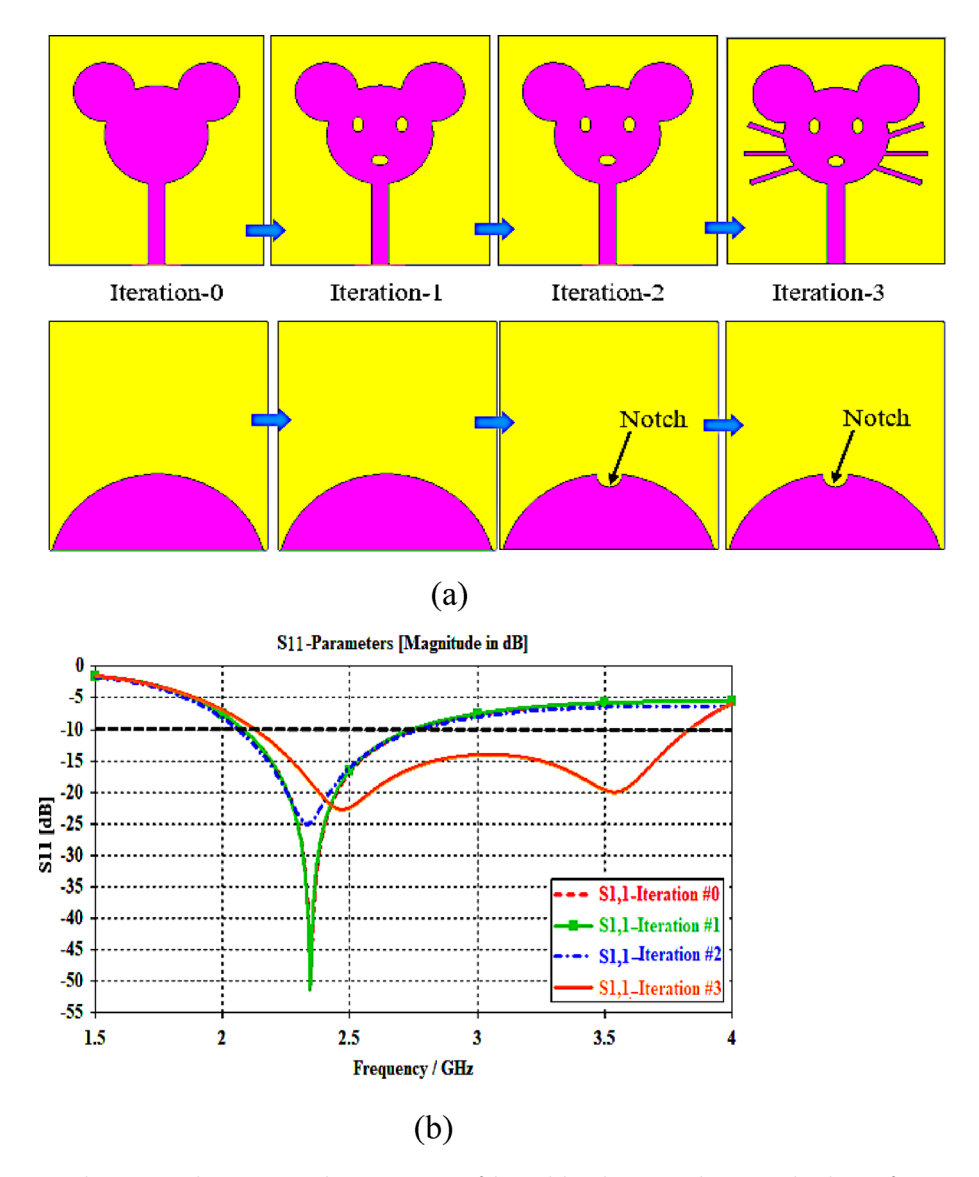


**Fig. 6** Showcases **a** the successive design iterations of the wideband antenna element in the shape of a mouse and **b** the simulated reflection coefficient  $S_{11}$  of the antenna across the four progressive design iterations

of  $f_t=2.51\,GHz$  and  $f_r=2.81\,GHz$ , respectively, are shown in Fig. 8(c). The two antenna input ports have computer-generated isolation levels of -30 dB at  $f_t$  and -35 dB at  $f_r$ . However, with values of S33 = -9 dB at  $f_t$  and S22 = -20 dB at  $f_r$ , the system shows comparatively low return losses.

# 3 Performance enhancement of the proposed duplexer using meandered transmission lines and DGS technique

In order to improve the isolation in the middle of port #2 and port #3, a DGS with an arc-shaped configuration is engraved into the ground plane. This separation is designed to isolate the ground of the antenna from the diplexer. This modification contributes to the ultimate arrangement of the recommended full-duplex Transmit/Receive (Tx/Rx) patch antenna system, illustrated in Fig. 9(a) and (b). The parameters of the simulated scattering for the finalized Tx/Rx antenna arrangement, incorporating meandered feeding transmission lines and the arc-shaped DGS, are presented in Fig. 9(c). It is noticed

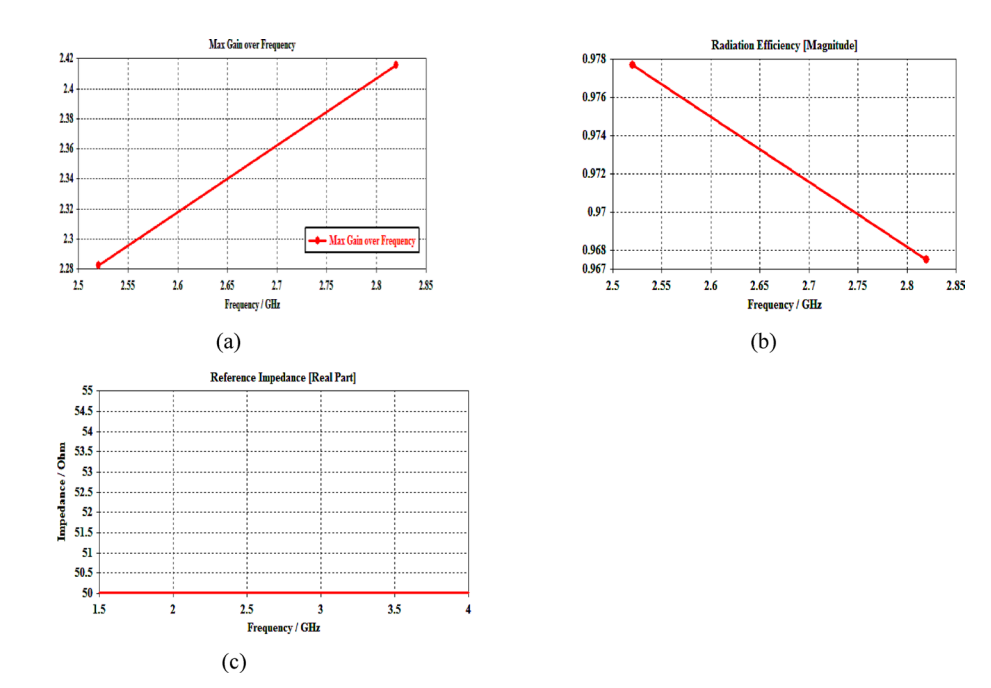


**Fig. 7** The virtual characteristics of the ultimate antenna configuration from iteration #3. **a** Antenna gain observed across different frequencies. **b** Efficiency, and **c** Reference impedance

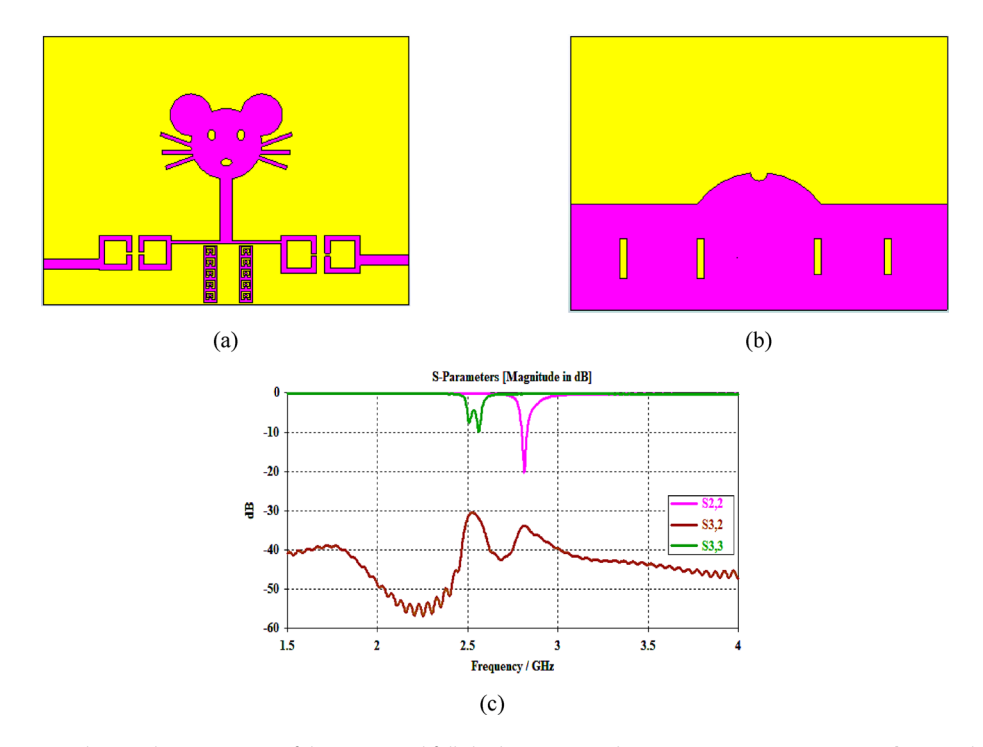


**Fig. 8** The initial arrangement of the suggested full-duplex Tx/Rx patch antenna structure: **a** top view, **b** ground plane and **c** the computer-generated scattering parameters

that the isolation between ports is significantly enhanced from -34~dB to -58~dB and from -27~dB to -31~dB at  $f_r=2.81~GHz$  and  $f_t=2.51~GHz$ , respectively as listed in Table 6.

The antenna's circular shape ensures a symmetric radiation pattern, making it well-suited for S-band communications. The inclusion of slots within the circular patch

Elabd et al. Discover Applied Sciences (2025) 7:1044 Page 15 of 21

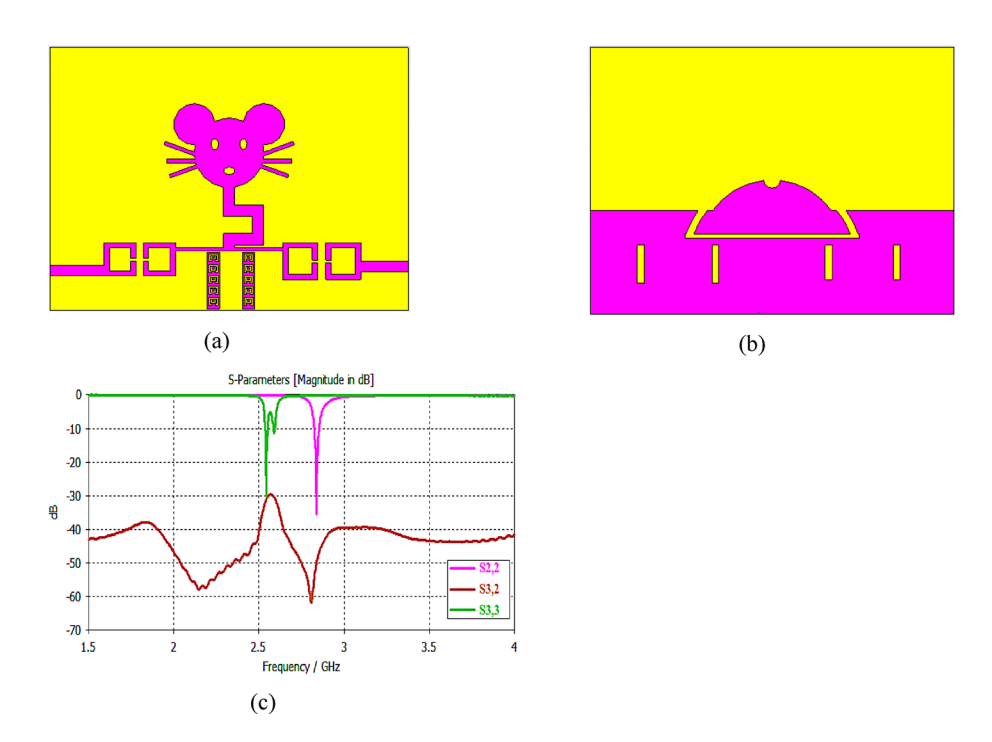


**Fig. 9** The completed scheme of the suggested full-duplex Tx/Rx patch antenna arrangement includes: **a** the view from top, **b** the ground plane, and **c** the simulated scattering parameters

**Table 6** The achieved performance characteristics of the optimized tx/rx antenna system, incorporating a meandered feeding transmission line and an arc-shaped DGS

C		D
Specifications	Тх	Rx
Size ( $mm^2$ )	$(100 \times 70) \ mm^2$	
$f_0$	$f_t = 2.51  GHz$	$f_r = 2.81  GHz$
FBW (%)	1.21%	1.7%
Reflection coefficient (dB)	$ s_{22}  = -32 dB$	$ s_{33}  = -38  dB$
Ports isolation (dB)	-31 dB	-58 dB

forming the Mickey Mouse shape serves to elongate the paths of surface currents, effectively leading to a lessening in the overall dimensions of the antenna.

Figures 10(a) and 10(b) present the simulated surface currents at  $f_t=2.51\ GHz$  and  $f_r=2.81\ GHz$ , respectively. As anticipated, the surface current is concentrated around the right SOLR at  $f_t=2.51\ GHz$  and the left SOLR at  $f_r=2.81\ GHz$ . To reduce coupling amid the two feeding ports, CSRR-shaped metamaterial-based BPFs are strategically placed near each SOLR to effectively trap currents in the undesired frequency bands, as illustrated in Fig. 10. Additionally, the fractional bandwidth (FBW) serves as an improved metric for comparing the bandwidth performance of different antennas. It is defined as the ratio of the absolute bandwidth, denoted as BW, to the center frequency  $f_0$ , as described in [1].

$$FBW\% = (BW/f_0) \times 100.$$
 (14)

Where BW is the transmit bandwidth  $BW_t$  and  $f_0=f_t$  for transmitting mode. While BW is the receive bandwidth  $BW_r$  and  $f_0=f_r$  for receiving mode. Thereby, the proposed duplexer has FBW=1.21~% and FBW=1.7~% at  $f_t=2.51~GHz$  and

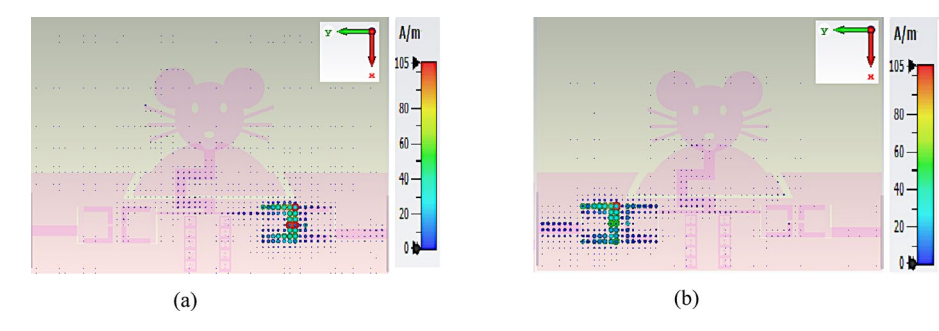


**Fig. 10** Simulated surface currents of The ultimate designed Tx/Rx antenna system using meandered feeding transmission line and the arc-shaped DGS: (a) at 2.51~GHz and (b) at 2.81~GHz

 $f_r = 2.81 \ GHz$ , respectively. It attains a compact frequency space ratio of r = 0.1127, as defined in [1].

$$r = |f_r - f_t| / (f_r + f_t) / 2 \tag{15}$$

This section showcases the simulated radiation patterns of the optimized Tx/Rx antenna system at the designated operating frequencies.

# 4 Measurements conducted in an experimental setting

The constructed model of the ultimate proposed Transmit/Receive (Tx/Rx) antenna system, employing meandered feeding transmission lines and the arc-shaped DGS, is depicted in Fig. 11(a) and (b). The Rohde & Schwarz ZVB 20 vector network analyzer (VNA) is employed to measure the scattering parameters of the system, as illustrated in Fig. 11(c). Figure 12 illustrates the dignified resonant frequencies at the transmitting and receiving ports, recorded at  $f_t = 2.51 \ GHz$  and  $f_r = 2.81 \ GHz$ , correspondingly. The measured isolation levels among the two input ports are  $-40 \ dB$  at  $f_t$  and  $-42 \ dB$  at  $f_r$ , surpassing the predected values of  $-31 \ dB$  and  $-58 \ dB$ , correspondingly.

A deviation between simulated and measured isolation is observed. This difference is mainly due to fabrication-related tolerances such as substrate thickness variation, photolithographic misalignment, and connector soldering imperfections. These practical effects are common in high-frequency prototypes and do not indicate a theoretical flaw in the design. Similar discrepancies have been reported in previous studies, confirming the robustness of the proposed structure. While the measured and simulated results show strong agreement, slight discrepancies can be attributed to fabrication tolerances.

The measured radiation patterns are performed using the reference gain horn antenna, Fig. 13 (a) show the schematic diagram of radiation pattern measurement setup. Figures 13(b) to 13(i) depict the computer-generated and measured normalized radiation patterns at  $\phi=0^\circ$ ,  $\phi=90^\circ$ ,  $\theta=90^\circ$  and  $\theta=0^\circ$  at  $f_t=2.51\,GHz$  and  $f_r=2.81\,GHz$ . Notably, at  $f_t=2.51\,GHz$ , the measured results exhibit a strong correlation with the computer-generated predictions, demonstrating high consistency between both datasets.

Elabd et al. Discover Applied Sciences (2025) 7:1044 Page 17 of 21

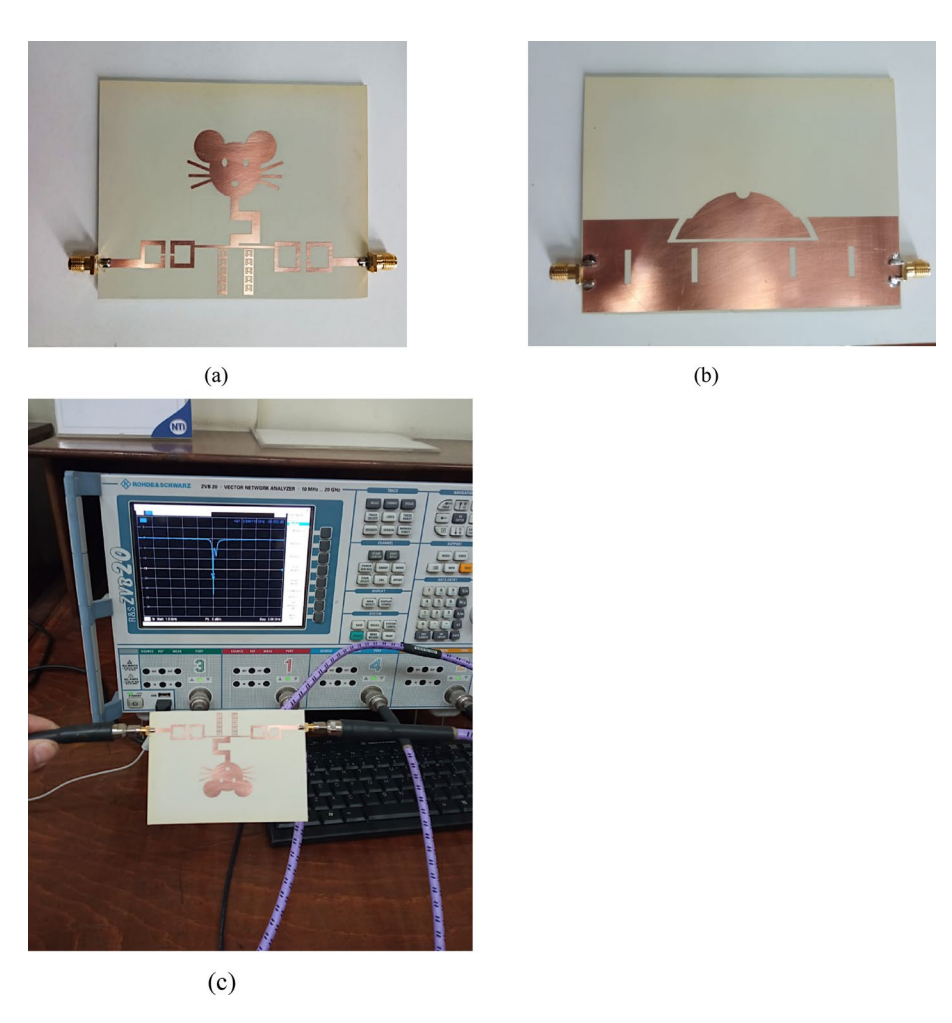


**Fig. 11** The finalized Tx/Rx antenna system is constructed using a meandered feeding transmission line and an arc-shaped DGS. The illustration includes  $\bf a$  the top view,  $\bf b$  the bottom view, and  $\bf c$  the measurement process conducted with the Rohde & Schwarz ZVB 20 VNA

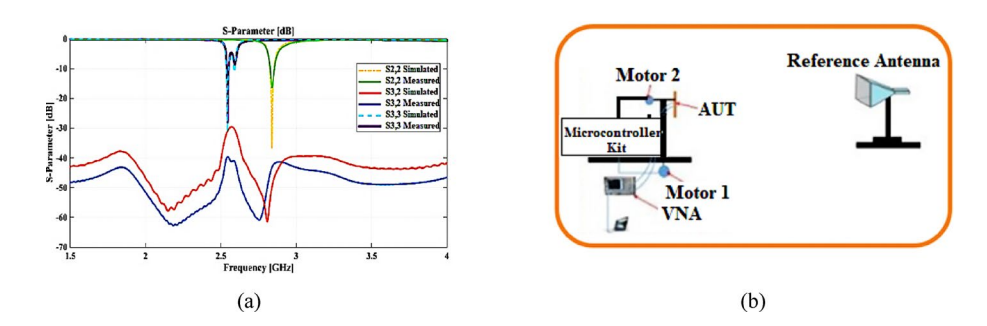


**Fig. 12** Predicted and measured S-Parameters of the final suggested Tx/Rx antenna system using meandered feeding transmission line and the arc-shaped DGS, and (b) the schematic diagram of radiation pattern measurement setup

# 5 Contrast with relevant studies

Table 7 summarizes the performance of recent diplexer designs in terms of size, operating frequency, fractional bandwidth (FBW), insertion loss, port isolation, return loss, and frequency spacing ratio. Compared to existing works, the proposed diplexer offers a balanced and superior performance. Notably, it achieves a compact size of  $0.4814 \, \lambda_0^2$ ,

Elabd et al. Discover Applied Sciences (2025) 7:1044 Page 18 of 21

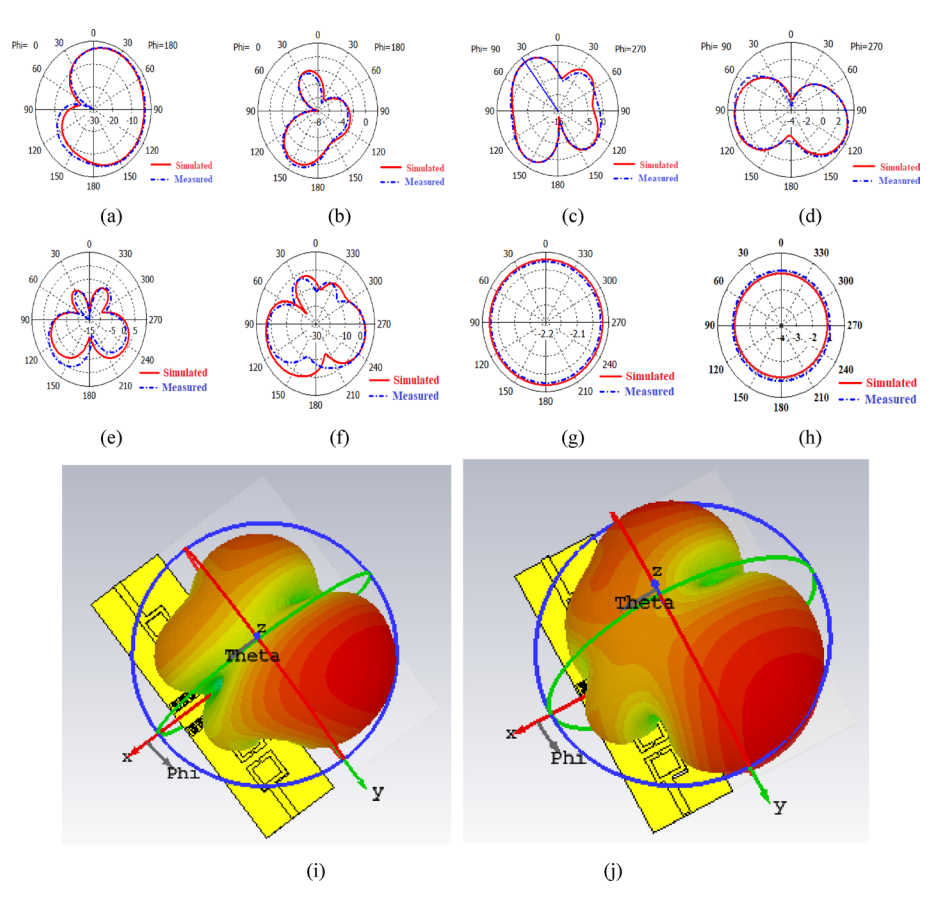


**Fig. 13** a the schematic diagram of radiation pattern measurement setup. The simulated and measured radiation patterns at  $\phi=0^\circ$  b  $f_t=2.51~GHz$ , c  $f_r=2.81~GHz$ , radiation patterns at  $\phi=90^\circ$  d  $f_t=2.51~GHz$ , e  $f_r=2.81~GHz$ , radiation patterns at  $\theta=90^\circ$  f  $f_t=2.51~GHz$ , g  $f_r=2.81~GHz$ , and radiation patterns at  $\theta=0^\circ$  h  $f_t=2.51~GHz$ , i  $f_r=2.81~GHz$ . i and j 3D radiation pattern of the final proposed system at  $f_t=2.51~GHz$  and  $f_r=2.81~GHz$ 

while maintaining low insertion losses of 1.09 dB at 2.51 GHz and 1.13 dB at 2.81 GHz. This performance is competitive with state-of-the-art compact designs such as [14] (0.87 dB, 0.0233  $\lambda_0^2$ ) and [34] (0.5 dB, 0.09  $\lambda_0^2$ ), while delivering significantly higher isolation of 31 dB and 58 dB, which surpasses most designs in the same frequency range, including [20] and [21]. Furthermore, the proposed work demonstrates a small frequency spacing ratio of 0.11278, which is better than many broadband or multi-band diplexers that often suffer from high ratios exceeding 0.2. Unlike many previous studies, this work also integrates the diplexer within a full-duplex antenna system, offering a complete and compact transceiver solution — a distinguishing factor from designs in [1–34] that focus solely on filter components. These enhancements clearly position the proposed diplexer as a high-performance candidate for modern full-duplex wireless communication systems.

Here,  $\,\lambda_{\,0}$  represents the free-space wavelength consistent to the lowest frequency in the operational band.

# **6 Conclusion**

This study presents innovative designs for a microstrip diplexer and a full-duplex antenna system, achieving superior isolation and minimal insertion loss. The proposed designs employ compact band-pass filters (BPFs) integrated with metamaterial-inspired

Elabd et al. Discover Applied Sciences (2025) 7:1044 Page 19 of 21

**Table 7** Comparison with related work

Ref	Size $\lambda_o^2$	Frequency (GHz)	FBW (%)	Insertion Loss (dB)	Isolation (dB)	Return Loss (dB)	Frequen- cy space ratio
[1]	0.3136	3.215/3.3	2.39	3/2.8	36/45	35/48	0.0245
[2]	0.735	1.98/2.55	3.9/5	NA	30	22/29	0.23
[3]	0.6889	3.9/4.9	NA	NA	34	32/38	0.227
[4]	0.4356	9/11.2	NA	NA	25	28/32	0.22
[5]	2.2	2.4/5.2	5.3/5.7	NA	20	12/20	0.74
[14]	0.0233	1.7/3.3	1.8	0.87	36	23/25	0.64
[15]	0.35	1.8/2.4	6/5.8	NA	30	20	0.286
[16]	1.2	2.2/2.6	4.55/5	1.6/1	40	22/30	0.167
[17]	4.6	8.04/9.07	4.23/4.19	2.35/2.33	49/53	30/38	0.12
[18]	1.5	1.81/2.03	2.25/3	1.98/1.9	58/46	28/30	0.114
[19]	0.167	1.8/2.1	5.5/6.2	2/1.8	40	20/19	0.154
[20]	0.89	1.85/2.5	NA	4.2/3.3	31	32/31	0.2988
[21]	0.98	1.41/2.02	NA	4.4/4.6	29	40/42	0.355
[22]	0.3	1.5/2.1	NA	1.5/1.8	45	32/30	0.333
[23]	3.5	9.5/10.6	6	2.6/2.3	45	35/32	0.1094
[24]	0.25	3.5/5	NA	1.5	25	20	NA
[25]	0.3	2.84/4.08	1.41/2.2	0.7/0.9	35	21.2/17	NA
[26]	0.08	0.895/2.2	NA	0.75/0.14	20.7	40/31	NA
[27]	0.33	6.7/8.4	NA	0.68/0.82	27	25	NA
[28]	0.35	2.6/6	NA	0.6/0.9	40	15	NA
[29]	0.004	0.9/1.8	21/24	NA	20	17/14	NA
[30]	0.435	2.191/2.584	1.24/0.64	1.2/1.79	21/21.9	32/41	0.1646
[31]	0.15	2.5	6.8	0.8	60	20	1.15
[32]	0.10	2.9	4.9	0.6	31	17	1.12
[33]	0.14	2.4	7.2	0.9	40	19	1.20
[34]	0.09	3.0	5.0	0.5	38	18	1.1
This work	0.4814	2.51/2.81	1.21/1.7	1.09/1.13	31/58	32/38	0.11278

techniques, including square open-loop resonators (SOLR), defected ground structures (DGS), and complementary square ring resonators (CSRR). These techniques significantly enhance the selectivity of the BPFs at the input ports of both the diplexer and the antenna system. In particular, the CSRR-based configuration effectively suppresses coupling effects, substantially improving isolation between the diplexer ports. Measured isolation levels between the diplexer ports reach -65 dB and -90 dB, with consistent fractional bandwidths of 2.5%. The corresponding insertion loss values are - 1.09 dB and -1.13 dB at the transmission ( $f_r$ =2.51 GHz) and reception ( $f_r$ =2.81 GHz) frequencies, respectively. Moreover, the diplexer is seamlessly integrated with a wideband Mickeyshaped patch antenna featuring a partially grounded structure, enabling bidirectional radiation. This integration results in an efficient full-duplex transceiver system, demonstrating isolation levels of -58 dB at 2.81 GHz and -31 dB at 2.51 GHz. The system also maintains a compact frequency spacing ratio of r = 0.11278. Its small form factor enhances practical applicability, making it suitable for real-world full-duplex communication systems requiring high performance. Future work will aim to extend the proposed design to support higher frequency bands relevant to 5G and emerging 6G technologies, integrate with MIMO architectures to enhance spatial diversity and channel capacity, and explore tunable or reconfigurable implementations to enable dynamic spectrum access in cognitive radio environments.

Elabd et al. Discover Applied Sciences (2025) 7:1044 Page 20 of 21

#### Acknowledgements

For their help in carrying out this project, the authors would like to thank the Ministry of Higher Education (MOHE) of Malaysia, the University Teknikal Malaysia Melaka (UTeM), and the New Damietta Higher Institute of Engineering and Technology (NDETI) in Damietta, Egypt.

#### **Author contributions**

R.H.Elabd and Amr H. Hussein, designed the diplexer and full-duplex antenna structure and conducted the simulations. A.J.A.Al-Gburi, provided technical guidance, enhanced the manuscript's scientific content, and contributed to the performance evaluation and experimental validation. All authors contributed to writing the manuscript and reviewed the final version.

## **Funding**

Not applicable.

# Data availability

No, I do not have any research data outside the submitted manuscript file.

#### Declarations

# Ethics approval and consent to participate

Not applicable.

#### Consent for publication

Not applicable.

#### **Competing interests**

The authors declare no competing interests.

Received: 18 April 2025 / Accepted: 25 June 2025

Published online: 22 September 2025

#### References

- Hussein AH, Abdullah HH, Attia MA, Abada AM. S-Band Compact Microstrip Full-Duplex Tx/Rx Patch Antenna With High Isolation. IEEE Antennas Wirel Propag Lett. 2019;18(10):2090–4.
- Xian JL, Ze MX, Pei SZ. Small Transmit-Receive frequency space filtering duplex patch antenna array with high isolation. Progress Electromagnet Res C. 2017;71:161–8.
- Althuwayb AA. Design of highly compact self-diplexing Y-shapedslot antenna employing quarter-mode substrate integrated waveguide. Int J RF Microw Comput Aided Eng. 2021. https://doi.org/10.1002/mmce.22827.
- Mukherjee S, Biswas A. Design of self-diplexing substrate integrated waveguide cavity backed slot antenna. IEEE Antennas Wirel Propag Lett. 2016;15:1775–8.
- Lee Y, Tarng J, Chung S. A filtering diplexing antenna for dual-band operation with similar radiation patterns and low cross-polarization levels. IEEE Antennas Wirel Propag Lett. 2017;16:58–61.
- Balani W, Sarvagya M, Samasgikar A, Ali T, Kumar P. Design and Analysis of Super Wideband Antenna for Microwave Applications. Sensors. 2021;21(2):477–92. https://doi.org/10.3390/s2102047.
- 7. Ammar AE, Mahmoud N, Ali MAA, Hussein Abdullah AH. Efficient diplexer with high selectivity and low insertion loss based on SOLR and DGS for wimax. Progress Electromagnet Res C. 2021;116:171–80.
- 8. Elabd RH, Al-Gburi AJA, Alhassoon K, Alsayaydeh JAJ, Saeidi T, Mohammed NJ, Zakaria Z. An ultra-selective OLR-based microstrip diplexer with minimal insertion loss for wireless communication system. Int J Intell Eng Syst. 2024;17(2):1.
- Al-Gburi AJA, Rahman NA, Zakaria Z, Palandoken M. Detection of Semi-Solid materials utilizing Triple-Rings CSRR microwave sensor. Sensors. 2023;23:3058. https://doi.org/10.3390/s23063058.
- 10. Baena JD, et al. Equivalent-circuit models for split-ring resonators and complementary split-ring resonators coupled to planar transmission lines. IEEE Trans Microwave Theory Tech. 2005;53(4):1451–61.
- Arora S, Sharma S, Anand R, et al. Integration of metamaterials for quintuple band-notched ultra-wideband antennas. Analog Integr Circ Sig Process. 2025;123:4. https://doi.org/10.1007/s10470-025-02355-7.
- 12. Selvaraju R, Jamaluddin MH, Kamarudin MR, Nasir J, Dahri MH. Complementary split ring resonator for isolation enhancement in 5G communication antenna array. Progress Electromagnet Res C. 2018;83:217–28.
- Shahzad W, Hu W, Ali Q, Raza H, Abbas SM, Lightnart LP. A Low-Cost Metamaterial Sensor Based on DS-CSRR for Material Characterization Applications. Sensors. 2022;22:2000–11. https://doi.org/10.3390/s22239087.
- Roshani S, Yahya SI, Mezaal YS, Chaudhary MA, Al-Hilali AA, Roshani A, Mojirleilani S. Design of a Compact Quad-Channel Microstrip Diplexer for L and S Band Applications. Micromachines. 2023;14:553–68. https://doi.org/10.3390/mi14030553.
- 15. Feng W, Gao X, Che W. Microstrip diplexer for GSM and WLAN bands using common shorted stubs. Electron Lett. 2014;50:1486–8. https://doi.org/10.1049/el.2014.2500.
- Tizya H, Riouch F, TRIBAK A. Microstrip diplexer design based on two square open loop bandpass filters for RFID applications. Int J Microw Wirel Technol. 2018;10(4):412–21. https://doi.org/10.1017/S1759078718000314.
- 17. Cheng F, Gu C, Zhang B. High isolation substrate integrated waveguide diplexer with flexible transmission zeros. IEEE Microwave Wirel Compon Lett. 2020;30(11):1029–32.
- Shaheen MM, Mahmoud NM, Alim A, Nasr ME, Hussien AH. Implementation of a Highly Selective Microstrip Diplexer with Low Insertion Loss Using Square Open-Loop Resonators and a T-Junction Combiner. Online. Radioengineering. 2022;31(3):357–361. ISSN 1210-2512. Dostupné z: https://doi.org/10.13164/re.2022.0357.
- FENG W. Microstrip diplexer design using open/shorted coupled lines. Progress Electromagnet Res Lett. 2016;59:123–7. https://doi.org/10.2528/PIERL16030805.

- 20. Hussein HA, Mezaal YS, Alameri BM. Miniaturized microstrip diplexer based on fr4 substrate for wireless communications. Elektronika Ir Elektrotechnika. 2021;27(5):34–40.
- 21. Chen CF, Zhou KW, Chen RY, Tseng HY, He YH, Li WJ, Weng JH. Design of microstrip multifunction integrated diplexers with frequency division, frequency selection, and power division functions. IEEE Access. 2021;9:53232–42.
- 22. Tahmasbi M, Razaghian F, Roshani S. Design of bandpass-bandpass diplexers using rectangular-, T-, and Lshaped resonators for hybrid power amplifier and 5G applications. Analog Integr Circuits Signal Process. 2021;109(3):585–97.
- Su ZL, Xu BW, Zheng SY, Liu HW, Long YL. High-isolation and Wide-stopband SIW diplexer using mixed electric and magnetic coupling. IEEE Trans Circuits Syst II Express Briefs. 2020;67(1):32–6.
- 24. Ben Haddi S, Zugari A, Zakriti A, Ouahabi ME, El Khamlichi D. Compact microstrip diplexer design using new octagonal resonators for 5G and Wi-Fi applications. J Instrum. 2023. https://doi.org/10.1088/1748-0221/18/03/P03033.
- Al-Majdi K, Mezaal YS. New miniature narrow band microstrip diplexer for recent wireless communications. Electronics. 2023;12:715. https://doi.org/10.3390/electronics12030716.
- Rezaei A, Yahya SI. A new design approach for a compact microstrip diplexer with good passband characteristics. ARO-The Sci J Koya Univ No. 2022. https://doi.org/10.14500/aro.10999.
- 27. Upadhyaya T, Pabari J, Sheel V, Desai A, R., and, Jitarwal S. Compact and high isolation microstrip diplexer for future radio science planetary applications. Int J Electron Commun (AEÜ). 2020;127:153497–504.
- 28. Noori L, Rezaei A. Design of a microstrip diplexer with a novel structure for wimax and wireless applications. Int J Electron Commun (AEÜ). 2017;77:18–22.
- 29. Rezaei, A., Yahya, S.I. & Nouri, L. An ultra-compact diplexer based on simple microstrip coupled lines for GSM and wideband wireless applications. Wireless Netw 30, 857–865 (2024). https://doi.org/10.1007/s11276-023-03519-x
- 30. Elabd RH, Hussein AH, Mousa ME. and A. A.Kabeel, Implementation of highly isolation OLR– Based microstrip Full-Duplex tx/rx antenna systems with low insertion loss for contemporary wireless system applications. EURASIP J Wirel Commun Netw. 2023.
- 31. Ben Haddi S, Zugari A, Zakriti A, Achraou S. High isolation microstrip bandpass diplexer for industry 4.0 communication. Microsystem Technologies. 2022;28(5):1167–78.
- 32. Mezaal YS, Khaleel SK, Alameri BM, Al-Majdi K, Al-Hilali AA. Miniaturized microstrip dual-channel diplexer based on modified meander line resonators for wireless and computer communication technologies. Technologies. 2024;12(5):57.
- 33. Hung C-M, Jheng C-F, Lee K-Y, Hsu C-IG, Ho M-H. Dual-band filter and diplexer design using extremely miniaturized substrate-integrated coaxial cavity. Sensors. 2025;25(9):2921.
- Elabd RH, Hussein AH, Mousa ME, Kabeel AA. Implementation of highly isolation open-loop resonators-based microstrip full-duplex Tx/Rx antenna systems with low insertion loss for contemporary wireless system applications. EURASIP Journal on Wireless Communications and Networking. 2024;2024;4.
- 35. Karimi Bavandpour S, Roshani S, Pirasteh A, Roshani S, Seyedi H. A compact lowpass–dual bandpass diplexer with high output ports isolation. AEÜ Int J Electron Commun. 2021;137:153748.
- 36. Roshani S, Dehghani K, Roshani S. A lowpass filter design using curved and fountain shaped resonators. Frequenz. 2019;73(7–8):267–72.
- 37. Roshani S, Koziel S, Roshani S, Jamshidi MB, Parandin F, Szczepanski S. Design of a patch power divider with simple structure and ultra-broadband harmonics suppression. IEEE Access. 2021;9:165734–44.

#### Publisher's note

Springer Nature remains neutral with regard to jurisdictional claims in published maps and institutional affiliations.